

Improved Equation-of-State Table of Deuterium for High-Energy-Density Applications

D. I. Mihaylov, V. V. Karasiev, S. X. Hu, J. R. Rygg, V. N. Goncharov, and G. W. Collins

Laboratory for Laser Energetics, University of Rochester

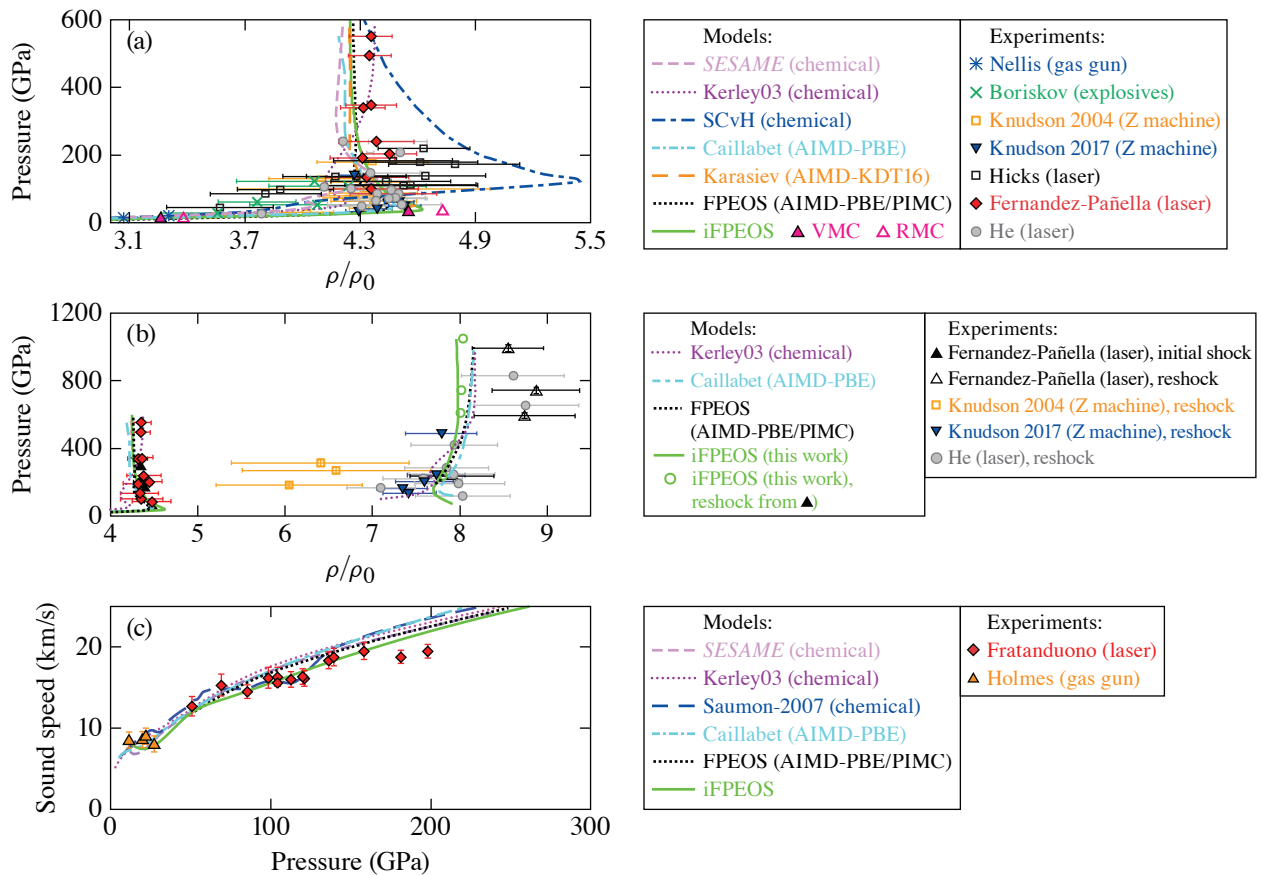
We present an improved first-principles equation-of-state (iFPEOS) table of deuterium that is an update on the previously established FPEOS table^{1,2} by introducing (1) fully consistent molecular dynamics (MD) driven by density functional theory (DFT) treatment for all ρ - T points, (2) a universal treatment of exchange-correlation (XC) thermal effects, and (3) quantum treatment of ions. This new iFPEOS includes ρ points in the range of $1 \times 10^{-3} \leq \rho \leq 1.6 \times 10^3 \text{ g/cm}^3$ and T points in the range of $800 \text{ K} \leq T \leq 256 \text{ MK}$, thereby covering the challenging warm-dense-matter regime.

For an improved description of the electronic structure at high T , iFPEOS employs newly developed T-SCAN-L (Ref. 3), which is a free-energy XC density functional with explicit temperature dependence at the meta-generalized gradient approximation (meta-GGA) level of DFT. Previous models such as FPEOS and other popular DFT-based models⁴ rely on the zero- T , GGA-level XC functional PBE (Perdew–Burke–Ernzerhof). Therefore, iFPEOS provides an improvement in accuracy by taking into account important XC thermal effects⁵ and including the higher-level, more-accurate treatment of the XC interaction. In addition, we combine T-SCAN-L with the rVV10 XC functional in order to account for van der Waals interactions. Recently, Hinz *et al.* demonstrated the success of DFT with SCAN-L+rVV10 XC in predicting the molecular dissociation boundary in dense D (Ref. 6). This accuracy of the SCAN-L+rVV10 functional, in combination with the development of T-SCAN-L, is the main motivation for constructing iFPEOS.

In the high- T regime, above $T \approx 250,000 \text{ K}$, standard Kohn–Sham (KS) DFT calculations become prohibitively expensive due to the high number of thermally occupied orbitals; therefore, we use orbital-free (OF) DFT. In OF DFT, the KS orbital-dependent kinetic energy functional is approximated by a density-dependent one. Here we use the newly developed noninteracting free-energy density functional LKTF γ TF, which is a one-parameter, tunable, convex combination of the Luo–Karasiev–Trickey free energy density functional (LKTF)⁷ and Thomas–Fermi functional. We tune the γ parameter and various densities spanning iFPEOS and also perform overlapping KS and OF calculations for T point in the region of switching from OF to KS in order to verify that results for pressure and energy agree to within 1% between the two methods.

Finally, nuclear quantum effects (NQE's) are accounted for via path-integral molecular dynamics (PIMD) calculations.⁸ Since PIMD calculations are much more computationally demanding, they are performed for only select ρ - T points for conditions in which NQE's are relevant. Results have been compared to those from classical MD and applied to the full iFPEOS as NQE's corrections. For computational details regarding KS, OF, and PIMD calculations, see Secs. III and IV in Ref. 9.

We compare iFPEOS to the latest results from experimental measurements of shock-compressed D, reporting principal and reshock Hugoniot¹⁰ and sound speed along the principal Hugoniot.¹¹ We performed an extra calculation at initial density $\rho_0 = 0.173 \text{ g/cm}^3$, $T = 19 \text{ K}$ so that initial conditions for solving the Rankine–Hugoniot equations are consistent with those reported in Ref. 10. The main conclusions from comparing the iFPEOS principal Hugoniot to experiment and other models is that iFPEOS provides an improvement in accuracy in the low-pressure ($P < 200 \text{ GPa}$), low- T regime ($T < 60,000 \text{ K}$), but at higher pressure and temperatures, the iFPEOS Hugoniot joins those predicted by other first-principles models that predict significantly lower compressibility [see Fig. 1(a)].



TC15795JR

Figure 1

(a) Pressure versus compression along the principal Hugoniot of shocked D as predicted by iFPEOS and other popular first-principles and chemical EOS models and calculations along with the latest experimental data. (b) Pressure versus compression in reshocked D. Collection of points and curves below compression of 5 is select principal Hugoniot data corresponding to (a). Data above compression of 5 correspond to latest experimental measurements along with various EOS models including iFPEOS reshock Hugoniot launched off of iFPEOS principal Hugoniot (solid green curve) and iFPEOS reshock states launched off of initial states corresponding to the ones reported in Ref. 10 (green circles) and determined via impedance matching with a-quartz. Green circles serve as a more direct comparison with latest experiments (black upright open triangles). (c) Sound speed along the principal Hugoniot as predicted by iFPEOS and other popular EOS models and according to latest experimental measurements. AIMD: *ab initio* molecular dynamics; KDT: Karasiev–Dufty–Trickey; PIMC: path-integral Monte Carlo; VMC: variational Monte Carlo.

Similar trends are seen in comparing iFPEOS reshock Hugoniot to experimental measurements [Fig. 1(b)], where for pressures $P > 600$ GPa, we see 6% to 11% underestimation of the compression in reshocked D. In the low-pressure regime of the reshocked Hugoniot, we see good agreement between different models that are all in good agreement with the latest experimental measurements considering the relatively larger error bars compared to measurements of principal Hugoniot. For $P > 600$ GPa, however, iFPEOS predicts even stiffer (1% to 3%) behavior than other models.

Finally, we compare iFPEOS to experimental measurements and other EOS model predictions of Eulerian sound speed along the principal Hugoniot [Fig. 1(c)]. This comparison further verifies the conclusions reached in Hugoniot comparisons, namely that iFPEOS provides slightly better agreement with experimental data in the low-pressure, low- T regime, but for $P > 200$ -GPa, iFPEOS, as well as other first-principles models, significantly disagrees with experiment by overestimating the sound speed. The excellent agreement with experimental gas-gun measurements at $P < 50$ GPa is expected since this is the region of molecular dissociation, which is accurately captured by the T-SCAN-L+rVV10 functional. The improved agreement with laser-shock

experimental data at $50 < P < 200$ GPa [red diamonds in Fig. 1(c)] is attributed to the improved treatment of XC thermal effects by T-SCAN-L, which are expected to be most important in these particular thermodynamic conditions ($20,000 < T < 80,000$ K).

This material is based upon work supported by the Department of Energy National Nuclear Security Administration under Award Number DE-NA0003856, U.S. National Science Foundation PHY Grant No. 1802964, the University of Rochester, and the New York State Energy Research and Development Authority.

1. S. X. Hu *et al.*, Phys. Rev. B **84**, 224109 (2011).
2. S. X. Hu *et al.*, Phys. Plasmas **22**, 056304 (2015).
3. V. V. Karasiev, D. I. Mihaylov, and S. X. Hu, “Meta-GGA Exchange-Correlation Free Energy Density Functional to Achieve Unprecedented Accuracy for Warm-Dense-Matter Simulations,” submitted to Physical Review Letters.
4. L. Caillabet, S. Mazevet, and P. Loubeyre, Phys. Rev. B **83**, 094101 (2011).
5. V. V. Karasiev, L. Calderín, and S. B. Trickey, Phys. Rev. E **93**, 063207 (2016).
6. J. Hinz *et al.*, Phys. Rev. Research **2**, 032065(R) (2020).
7. K. Luo, V. V. Karasiev, and S. B. Trickey, Phys. Rev. B **101**, 075116 (2020).
8. M. Ceriotti *et al.*, J. Chem. Phys. **133**, 124104 (2010).
9. D. I. Mihaylov *et al.*, Phys. Rev. B **104**, 144104 (2021).
10. A. Fernandez-Pañella *et al.*, Phys. Rev. Lett. **122**, 255702 (2019).
11. D. E. Fratanduono *et al.*, Phys. Plasmas **26**, 012710 (2019).